Surface & Coatings Technology 421 (2021) 127446

Contents lists available at ScienceDirect

Surface & Coatings Technology

journal homepage: www.elsevier.com/locate/surfcoat

Effects of strontium-substitution in sputter deposited calcium phosphate coatings on the rate of corrosion of magnesium alloys

Jonathan G. Acheson [a], Stephen McKillop [a], Joanna Ward [a,*], Abhijit Roy [b], Zhigang Xu [c], Adrian R. Boyd [a], Patrick Lemoine [a], Prashant N. Kumta [b,d,e,f], Jagannathan Sankar [c], Brian J. Meenan [a,*]

[a] Nanotechnology and Integrated Bioengineering Centre (NIBEC), School of Engineering, Ulster University, Shore Road, Newtownabbey, Co Antrim BT37 0QB, Northern Ireland, UK
[b] Department of Bioengineering, University of Pittsburgh, Pittsburgh, PA 15261, USA
[c] Department of Mechanical Engineering, North Carolina A&T State University, Greensboro, NC 27411, USA
[d] Department of Chemical and Petroleum Engineering, University of Pittsburgh, Pittsburgh, PA 15621, USA
[e] Department of Mechanical Engineering and Materials Science, University of Pittsburgh, Pittsburgh, PA 15621, USA
[f] Centre for Complex Engineered Multifunctional Materials, University of Pittsburgh, Pittsburgh, PA 15621, USA

ARTICLE INFO

Keywords:
Strontium-substituted calcium phosphate coatings
RF magnetron sputter deposition
Magnesium alloys
Corrosion rate
Micro-computed tomography (μCT)

ABSTRACT

Magnesium (Mg) alloys have significant potential for use as bioresorbable orthopaedic implant devices due to their controllable mechanical properties and an ability to promote new bone growth. However, difficulty lies with controlling the rate of corrosion in physiological conditions to ensure the load-bearing capability of the device is maintained for the required period of time, specifically until an adequate quantity of new bone tissue is formed. In this work, RF magnetron sputtering has been used to create calcium phosphate (CaP) and strontium-substituted calcium phosphate (SrCaP) thin film coatings on two Mg alloy systems (denoted WJK and ZEWX) that have been formulated for the fabrication of orthopaedic fracture fixation devices. A 14-day static-dynamic immersion study in simulated body fluid (SBF), shows that uncoated WJK substrates had a corrosion rate of 4.04 ± 0.15 millimetres per year (mmpy), which was reduced to 3.22 ± 0.17 mmpy with the application of a CaP coating, and to 2.92 ± 0.05 mmpy with a SrCaP coating. Uncoated ZEWX substrates had a corrosion rate of 3.36 ± 0.05 mmpy which was reduced to 2.98 ± 0.19 mmpy and 2.79 ± 0.03 mmpy, for CaP and SrCaP coatings, respectively. Whereas the sputter-deposited CaP and SrCaP coatings completely dissolve in SBF over the period of immersion, their presence at the outset significantly decreases the corrosion rate of both Mg alloys, as compared to the values for the uncoated substrates. Successful incorporation of Sr within the coating offers the potential for improved bioactivity with respect to directing the bone cell response to create new tissue.

1. Introduction

Magnesium (Mg) offers unique properties for the fabrication of resorbable orthopaedic fracture fixation devices due to its mechanical properties, with a Young's Modulus (41–45 GPa) similar to that of native human bone (3–20 GPa). Additionally, it provides for non-toxic biodegradability within the body. However, if this degradation takes place prematurely it can result in failure of any attendant orthopaedic load bearing device. For example, Boland et al. have reported that a rate of corrosion of 3.5% reduces the cyclic loading capability of a Mg medical device by a factor of 16 [1]. Two main approaches have been developed to improve the corrosion resistance of Mg, namely (1) tailoring composition and/or microstructure by alloying [2–4] or (2) coating with a barrier material [5–7].

Alloying of Mg with a range of other chemical elements has been widely reported [8,9], with studies showing significant improvements in both mechanical strength and corrosion resistance [10,11]. Commercial Mg alloys such as AZ31 and AZ91 have been widely used as model systems for biomedical applications, however, as they are not specifically designed for implant biodevices, their biocompatibility can be a

Abbreviation: CaP, Calcium phosphate; SrCaP, strontium-substituted calcium phosphate; SBF, simulated body fluid; μCT, micro-computed tomography.

* Corresponding authors.
E-mail addresses: je.ward@ulster.ac.uk (J. Ward), bj.meenan@ulster.ac.uk (B.J. Meenan).

https://doi.org/10.1016/j.surfcoat.2021.127446
Received 30 March 2021; Received in revised form 16 June 2021; Accepted 17 June 2021
Available online 24 June 2021

problem due to the presence of aluminium which has been linked to muscle fibre damage and a decrease in osteoclast viability [12–14]. Novel Mg alloys, formulated with the inclusion of copper, zinc and strontium can provide for negligible cytotoxicity and targeted mechanical properties.

In order to increase metal and/or alloy corrosion resistance, a protective coating can be applied using a range of techniques including plasma spraying [15,16], sol gel [17–19], micro arc oxidation technology [20–22] and RF magnetron sputtering [23–26]. In the case of a normal orthopaedic implant device, barrier layers can be used to negate any interaction between the underlying Mg and body fluids [6,27] whereby Cl^- ions will actively promote degradation. In addition to providing for corrosion resistance, such coatings can also influence the response to the surrounding biological environment by way of enhancement of biocompatibility, bioactivity, or drug/biologic delivery [28,29]. However, in circumstances where the expectation is that the Mg alloy implant device will, by design, undergo *in vivo* bioresorption, the associated coating will need to do likewise. To this end, rather than acting as a barrier to corrosion, the coating needs to undergo dissolution at a slower rate than the Mg alloy thereby controlling its gross degradation. In addition, as reported previously [25], ions released from the coating can work in tandem with those resulting from the degradation of the Mg alloy to regulate attendant cell/tissue response.

Calcium phosphate (CaP) coatings based on hydroxyapatite (HA) and its various chemical analogues, have been studied widely for various biomedical applications due to their inherent bioactivity [30,31]. These coatings contain elements that are similar to those present in the mineralized inorganic phase of native human bone [32,33] and can promote new tissue growth leading to provision of long-term *in vivo* stability. Several orthopaedic implant systems currently rely on such coatings to promote an improved osteoconductive response. In this regard, the release of Ca^{2+} and PO_4^{3-} ions facilitates the formation of cellular interactions on the implant surface that can then directly promote bone regeneration. RF magnetron sputtering has been used extensively to produce well-adhered HA-like CaP coatings on a range of metal substrates [24,34–37]. These coatings are referred to as being CaP due to the Ca^{2+} and PO_4^{3-} stoichiometric ratio being slightly different to that of the HA target material. Previous studies have shown that such sputter deposited CaP coatings can delay corrosion of Mg alloys while still undergoing dissolution [38]. The use of substituted hydroxyapatite systems, including those with single and multiple ions such as zinc (Zn^{2+}), fluoride (F^-), silver (Ag^+) and strontium (Sr^{2+}) [26,39–41] replacing calcium (Ca^{2+}) in the HA lattice, offers the potential to create coatings that can both control Mg alloy corrosion and attendant enhanced bioactivity with the potential for conferring an osteoinductive response. Strontium plays an important role in bone formation, with Sr^{2+} ions stimulating osteoblastic cell proliferation and differentiation [42–44]. *In vitro* response to Sr^{2+} is dose-dependent, with 3–7% significantly stimulating osteoblast differentiation [12], while 1% is sufficient to reduce osteoclast proliferation [45,46]. Previous studies have investigated the amount of incorporation of Sr^{2+} within different metal substrates [24,39] and its use to control the corrosion of Mg and its alloys [47–49]. However, the effects on Mg alloy corrosion rate of SrCaP coatings deposited by RF magnetron sputtering have not yet been reported.

In this work, CaP and SrCaP coatings have been deposited by RF magnetron sputtering onto two novel medical grade Mg alloys and their effects on corrosion rate measured utilising a static-dynamic immersion method [50]. Scanning Electron Microscopy (SEM) with Energy Dispersive Analysis (EDX) and Time-of-Flight Secondary Mass Spectrometry (ToF-SIMS) have been used to determine coating composition. Micro-Computed Tomography (μCT) has been employed to determine substrate volume loss and associated gravimetric analysis to calculate corrosion rate.

2. Material and methods

2.1. Sample preparation

Customised magnesium alloys, namely ZEWX (square coupons, 10 mm × 10 mm × 1.6 mm) and WJK (discs, diameter (□) 10 mm × 1 mm) coupons were manually abraded using *SiC* paper up to grade p1200 and cleaned using 99% isopropyl alcohol (Sigma Aldrich, UK). Abraded coupons were then dried and stored in a desiccator at 30% relative humidity until required.

Alloy composition is detailed in Table 1. The ZEWX synthesis procedure and composition have been reported previously [51]. The cast alloy went through a solution heat treatment before being used for coating studies. Heat treatment process included a first step of soaking at 320 °C for 10 h and then an additional one at 510 °C for 10 h followed by quenching in oil. The heat treatment operation was performed in an argon environment. The WJK alloy was prepared in a similar way and its actual composition verified by inductively coupled plasma optical emission spectroscopy (ICP-OES, iCAP duo 6500 Thermo Fisher, Waltham, MA). Standard solutions with known different concentrations of Mg, Sr, Y, and Zr were prepared using certified single element standard solutions suitable for ICP (Sigma-Aldrich, St. Louis, MO). Deionized water was used as blank standard. 100 mg of the alloy was cut from the extruded rod and dissolved in 40 mL of 5% nitric acid. The resultant solution was then diluted to analyse the elemental concentrations.

Sputter targets were fabricated using a dry press method whereby 11.5 g of either HA (Plasma Biotal Captal-R, UK) or Sr-HA (13 at.% of Sr biphasic calcium phosphate, Himed Inc. NY, USA) powders were pressed into the recessed copper backing plates using a stainless-steel die within a hydraulic press at a maximum applied load of 80 kN for 30 s. The pressed, targets were wrapped in aluminium foil and stored in a drying oven at 60 °C prior to being loaded into the RF magnetron sputtering system.

2.2. RF magnetron sputtering

Deposition of CaP and SrCaP coatings onto abraded ZEWX and WJK Mg alloy coupons was carried out in a custom-built high vacuum sputtering system that has been described in detail elsewhere [24]. In brief, the coating chamber comprises two Torus™ magnetron sources (Kurt J Lesker, USA), each arranged at an incident angle of 45° with respect to the sample holder platform located above. Each source is powered by an RF supply operating at 13.56 MHz with an automated matching air capacitor network (Huttinger, GmbH, Germany) placed between the RF supply and the source to reduce any reflected power to close to zero. Coatings were deposited on both sides of the substrates, across two sputter runs, using the parameters shown in Table 2.

The Mg alloy coupons were attached to the rotating sample holder located 100 mm above the sputter target sources *via* high vacuum carbon tape. Upon completion, carbon tape was physically removed, and any residue was removed using a cotton swab and isopropyl alcohol. Substrates were thoroughly dried prior to the second sputter run, to coat the remaining face. A ramp up power of 1 W/s was used for CaP targets,

Table 1
Elemental composition (wt%) of ZEWX and WJK Mg alloys.

	ZEWX (wt %)	WJK (wt %)
Magnesium (Mg)	97.1	97.5
Zinc (Zn)	1.0	–
Rare-earth metals: neodymium and gadolinium (Nd/Gd)	1.0	–
Zirconium (Zr)	0.3	0.5
Yttrium (Y)	0.3	1.0
Calcium (Ca)	0.3	–
Strontium (Sr)	–	1.0

Table 2
RF Magnetron sputtering conditions used to coat abraded ZEWX and WJK Mg alloys.

	CaP	SrCaP
Power (W)	150	150
Ramp up power (W/s)	1	0.2
Time (hours)	30	30
Chamber pressure (mbarr)	5 × 10–5	5 × 10–5
Working gas	Argon	Argon
Gas flow rate (standard cubic cm/min)	32–35	32–35
Throw distance (mm)	100	100

however, due to the fragile nature of the SrCaP target the ramp up power was reduced to 0.2 W/s, to prevent surface cracking. RF magnetron sputtering was undertaken using dry pressed powder targets for a period of 30 h using the conditions provided in Table 2. Thin film CaP coating thickness has been related to sputtering parameters on a range of substrates [24,26,34,36]. More specifically, on magnesium, the parameters used in Table 2 are known to yield a CaP and SrCaP coating thickness of ~340 nm based on previous studies of the relationship between film thickness and sputter time, carried out using ToF-SIMS depth profiling and contact profilometry [25]. Sputter deposited CaP and SrCaP coatings are commonly referred to as being "as-deposited" to note that they have not been subjected to any post-deposition treatment. As this is the case in throughout this work, samples are henceforth referred to as CaP and SrCaP coatings.

2.3. Static/dynamic corrosion testing

Corrosion testing was carried out by immersion of samples in simulated body fluid (SBF) [52,53]. Table 3 shows the concentration of ions present in the SBF used here, with those in blood plasma provided for comparison. Coupons of each Mg alloy with and without CaP or SrCaP coatings were submerged in 15 mL of SBF solution and incubated at 37 °C under atmospheric pressure conditions for a total period of 14 days with the SBF solution being replaced daily. Mg alloys were fully immersed into SBF with the edges left unsealed. This method constitutes a static-dynamic approach which seeks to, in part, represent the fluid exchange that occurs under physiological conditions and to prevent ion exhaustion of biogenic ions [54]. A representative set of samples ($n = 5$) for each Mg alloy were subject to the static/dynamic corrosion testing over the 14-day period, before being removed from the test solution and subject to post-immersion characterisation. A small amount of hydrogen gas evolution was observed throughout the course of the 14-day immersion study but did not cause any adverse effects.

The corrosion by-products created on Mg coupon surfaces after exposure to SBF were removed post-immersion at each time point in accordance with details in ASTM G01-0351 [55]. Corrosion rates were then calculated in millimetre/year (mmpy) using Eq. (1):

$$Corrosion\ Rate = \frac{KW}{ATD}, \quad (1)$$

where:K is a constant value (8.76×10^4);W represents mass loss (g);A is the nominal surface area (cm^2);T is exposure time in media (hours);D represents material density (g/cm^3).

Table 3
Ion concentration profile for SBF compared to blood plasma.

	SBF (mmol/L)	Blood plasma (mmol/L)
Na^+	142.0	142.0
K^+	5.0	5.0
Mg^{2+}	1.5	1.5
Ca^{2+}	2.5	2.5
Cl^-	148.8	103.0
$H_2PO_4^-$	1.0	1.0
SO_4^{2-}	0.5	0.5
HCO_3^-	4.2	27.0

Samples were subjected to gravimetric analysis pre- and post-corrosion testing based on the weight loss measured using 4Y precision scales (Radwag, Poland). Individual coupon weight was measured in grams with an accuracy to 6 decimal places and these values were then used to determine the mass loss (W) in the corrosion rate Eq. (1).

2.4. Surface characterisation

Scanning electron microscopy with Energy Dispersive X-Ray (SEM-EDX) was carried out using a Hitachi SU5000 (Hitachi, Japan) microscope equipped with an X-Max silicon drift detector (SDD) (Oxford Instruments, UK). SEM images were acquired at 10 keV with a nominal spot size of 50 nm, with EDX analysis undertaken under the same conditions with 5 frames/map recorded at a resolution of 1024 × 1024. The resulting elemental analysis was used to determine the Ca/P ratio for coatings on each Mg alloy type. As the conditions used to deposit the CaP and SrCaP coatings onto all of the alloy samples were the same, pre-immersion SEM-EDX data were obtained here for the ZEWX alloy samples only.

Time-of-Flight Secondary Ion Mass Spectrometry (ToF-SIMS) was undertaken using an IONTOF-5 instrument (IONTOF GmbH, Germany) equipped with a Bismuth (Bi) liquid metal ion gun, operating with the primary Bi+ ion species at a beam energy of 25 keV. Positive polarity mapping was completed across an area of 250 × 250 μm with 1024 × 1024 pixels per ion map, at a target current of 1 μA. Datasets were collected over 5 scans for each area imaged at a cycle time of 100 μs to allow for analysis at a suitable resolution. ToF-SIMS analysis was carried out for CaP and SrCaP coatings ZEWX alloys only and are deemed representative of those on WKJ alloys.

Micro-Computed Tomography (μCT) analysis was carried out on a SkyScan 1275 μCT instrument (Bruker, Germany) with X-rays created at an operating voltage of 40 kV and current of 250 μA. The image voxel size was 10 μm^3 and X-ray images were created as individual slices using the NRecon software package (Bruker, Germany). These slices were then subject to thresholding to identify the Mg alloy material before pixel thresholding analysis was run to determine the volumetric metrics using CTAn software (Bruker, Germany). Volume loss was calculated as a percentage of pre-immersion alloy volumes. All the scans were performed and evaluated under the same operating conditions to allow for direct comparison between the various sample sets. Volumetric images were produced using the rendering routines within the CTAn software. It is noted that the error associated with volume loss measurements was obtained by averaging across $n = 5$ samples.

3. Results

Scanning Electron Microscopy with Energy Dispersive X-Ray (SEM-EDX) analysis was used to determine the chemical composition of the CaP and SrCaP coatings deposited on the ZEWX Mg alloy, pre-immersion in SBF. SEM images of the ZEWX alloy samples before and after CaP thin film coating are shown in Fig. 1. The pristine Mg alloy (Fig. 1(a)) has been conditioned with p1200 abrasive paper to create a more uniform surface finish prior to coating and causes the formation of randomly oriented striations (Fig. 1(b)). High magnification SEM images for the uncoated alloy surfaces again show the striations on the abraded Mg alloy (Fig. 1(c) and (d)), whereas the CaP coated substrates have a pronounced globular topography (Fig. 1(e) and (f)). These latter high magnification SEM images show no evidence of defects or areas of delamination of the sputter deposited CaP suggesting the presence of a well adhered coating on the alloy surface. Data from EDX analysis of these surfaces is presented as percentage atomic concentration (at. conc. (%)) values in Table 4, along with the respective Ca/P and Ca+Sr/P ratios. X-ray spectral data from EDX analysis of the CaP and SrCaP coatings on the ZEWX Mg alloy, pre-immersion in SBF, is shown in Fig. 2. The key elements detected for CaP are magnesium (Mg),

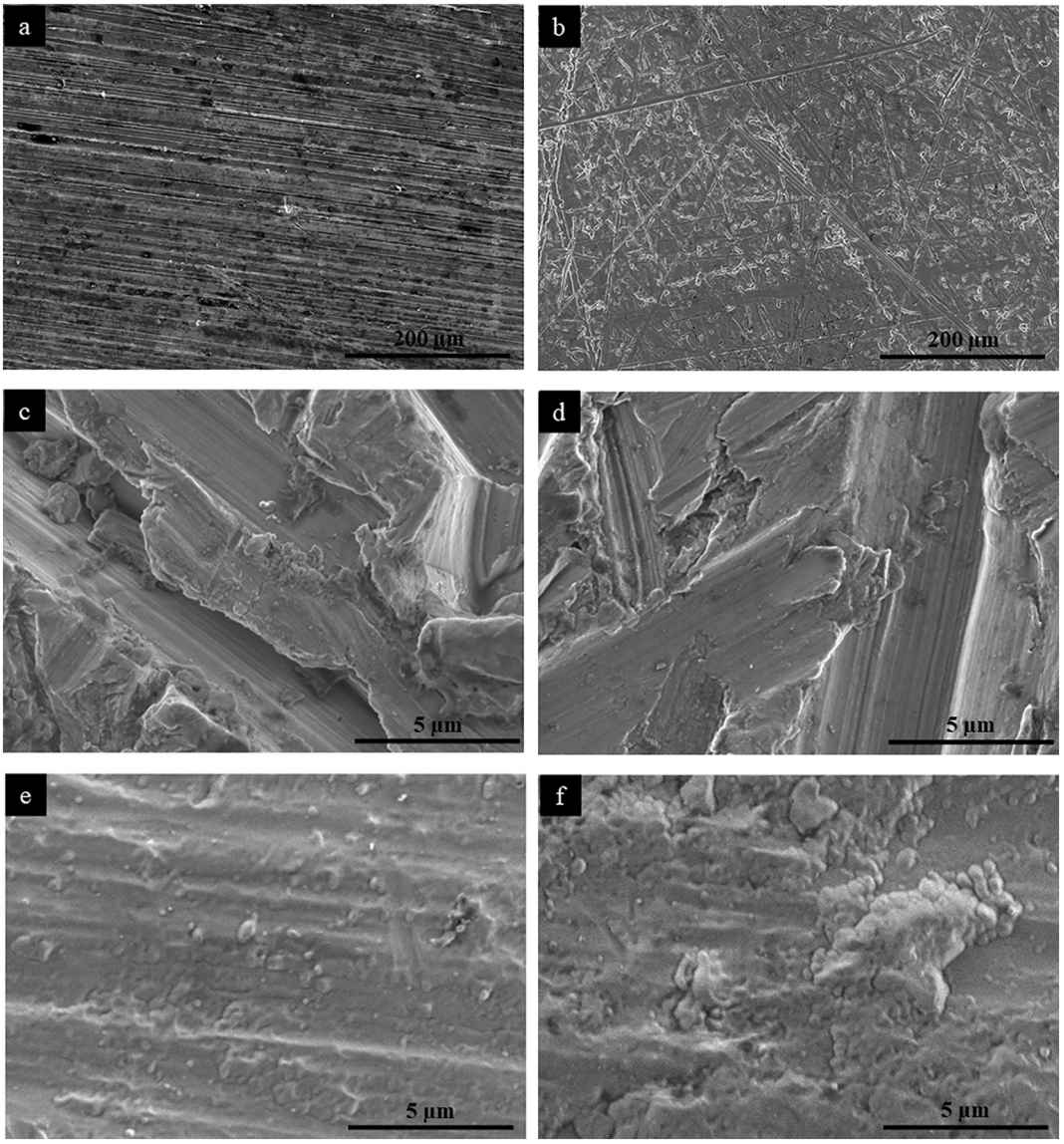

Fig. 1. SEM images for ZEWX alloy (mag ×200) (a) in the pristine state, (b) after conditioning with p1200 abrasive paper. Scale bar = 200 µm. High magnification (×10k) images for(c) – (d) uncoated Mg alloy (e) – (f) with CaP sputter coating. Scale bar = 5 µm.

Table 4
Atomic concentration (at. conc. (%)) values determined by SEM-EDX analysis for CaP and SrCaP coatings on ZEWX Mg alloys, pre-immersion in SBF.

Element	CaP	SrCaP
Oxygen	41.7 ± 0.2	41.7 ± 1.2
Carbon	4.0 ± 0.1	10.2 ± 0.67
Phosphorus	9.8 ± 0.0	8.6 ± 0.4
Strontium	0.0 ± 0.0	2.5 ± 0.1
Calcium	14.7 ± 0.1	11.0 ± 0.2
Magnesium	29.8 ± 0.2	26.0 ± 2.5
Sodium	[a]	[a]
Ca/P ratio	1.50	1.28
Ca+Sr/P	–	1.56

[a] Trace amounts of element.

phosphorous (P) and calcium (Ca). The presence of a significant amount of oxygen (O) in the EDX analysis is attributed to its presence in the phosphate groups (PO_4^{3-}) within both CaP and SrCaP coatings, while the carbon (C) contribution is deemed to be due to adventitious carbon present on the substrate surface. The addition of strontium (Sr) reflects the change in the SrCaP coating material.

ToF-SIMS analysis was used to further determine the surface chemistry of the CaP and SrCaP coatings. Positive polarity maps collected for CaP and SrCaP coated ZEWX Mg alloy substrates only, are displayed in Figs. 3 and 4, respectively. The total, sum of the rest and individual ion count maps for the CaP coated ZEWX Mg alloy (Fig. 3) show striation patterns which are accredited to the manual abrasion technique employed. However, this does not significantly influence the distribution of the $CaOH^+$ and Ca^+ ions, which are present in high amounts across the 250 × 250 µm raster area. $SrOH^+$ and Sr^+ maps have also been included here to confirm the absence of strontium within the coating.

The corresponding pseudo-colour ToF-SIMS images for the SrCaP coated ZEWX alloy again show the presence of striations due to abrasion of the pristine Mg alloy (Fig. 4). The $CaOH^+$ and Ca^+ ion counts detected here are similar to those for the CaP coating. Signals associated with $SrOH^+$ and Sr^+ ions are now clearly present across the surface confirming the presence of the expected Sr component in the CaP coating.

Rendered volumetric µCT images for the WJK alloy, with and without CaP and SrCaP coatings, after immersion in SBF for 14 days, are shown in Fig. 5. After exposure to SBF, each substrate clearly shows a pitted topography which reflects the normal mechanism for corrosion of Mg alloys. However, on closer inspection it is clear that the CaP and

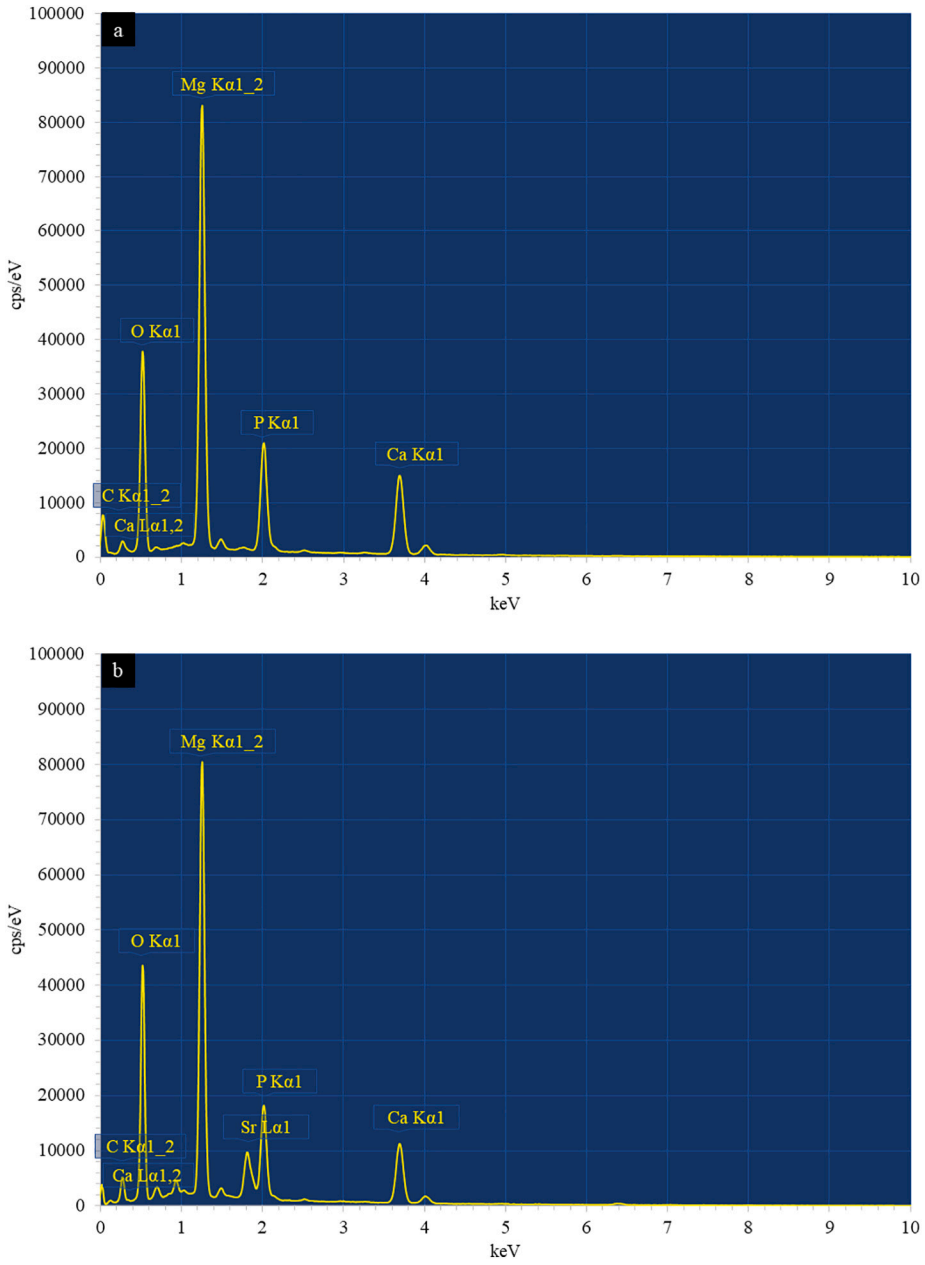

Fig. 2. X-ray spectra derived from SEM-EDX analysis for (a) CaP and (b) SrCaP coated ZEWX Mg alloys, pre-immersion in SBF.

SrCaP coated substrates (Fig. 5c, d) have undergone less pitting than the pristine Mg alloy (Fig. 5b) which implies that the presence of the coating provides a degree of resistance to the corrosion process.

The corrosion rate for each of these post-immersion samples, as calculated by gravimetric analysis, is provided in Fig. 6. These data indicate that the uncoated WJK Mg alloy has a 14-day corrosion rate of 4.04 ± 0.15 mmpy. By comparison, both the CaP and SrCaP coated WJK substrates show a statistically significant ($p < 0.001$) reduction in the corrosion rate with values of 3.22 ± 0.17 and 2.92 ± 0.05 mmpy, respectively. There is no statistically significant difference in corrosion rate between the SrCaP and CaP coated WJK samples.

The change in total volume for each Mg alloy (WJK and ZEWX), with and without CaP and SrCaP coatings after immersion in SBF for 14-days are provided in Table 5. The pristine WJK alloy is found to have a volume loss of ~40.3% of its original value (71.2 ± 3.8 mm^3) whereas both the CaP and SrCaP coated alloys also showed a considerably lower loss in volume, which in both cases was 29.1%.

The rendered volumetric μCT images for the ZEWX Mg alloy, with and without CaP and SrCaP coatings, before and after immersion in SBF for 14 days are shown in Fig. 7. After exposure to SBF, the uncoated ZEWX alloy clearly shows major areas of loss of material around the perimeter (Fig. 7b) of the substrate which translates to a reduction in volume by 20.9 ± 12.8% from that of the pre-immersion volume (161.1 ± 16.4 mm^3). By comparison, the CaP coated alloy surface shows much less loss of material (7.9 ± 8.1%) but has clear regions of extensive pitting across the face of the coupon. Likewise, the SrCaP coated sample (Fig. 7d) shows pronounced pitting occurring across the surface but to a lesser extent than for the CaP coated ZEWX.

Gravimetric analysis data for these samples has again been used to calculate corrosion rate, with values shown in Fig. 8. The uncoated ZEWX Mg alloys have a corrosion rate of 3.36 ± 0.05 mmpy while the presence of both CaP and SrCaP coatings on this substrate surface significantly reduces the corrosion rate to values to 2.98 ± 0.19 ($p < 0.1$) and 2.79 ± 0.03 mmpy ($p < 0.001$), respectively.

SEM images for CaP and SrCaP coated WJK and ZEWX alloy samples post-immersion in SBF for 14 days are shown in Fig. 9. The coatings have

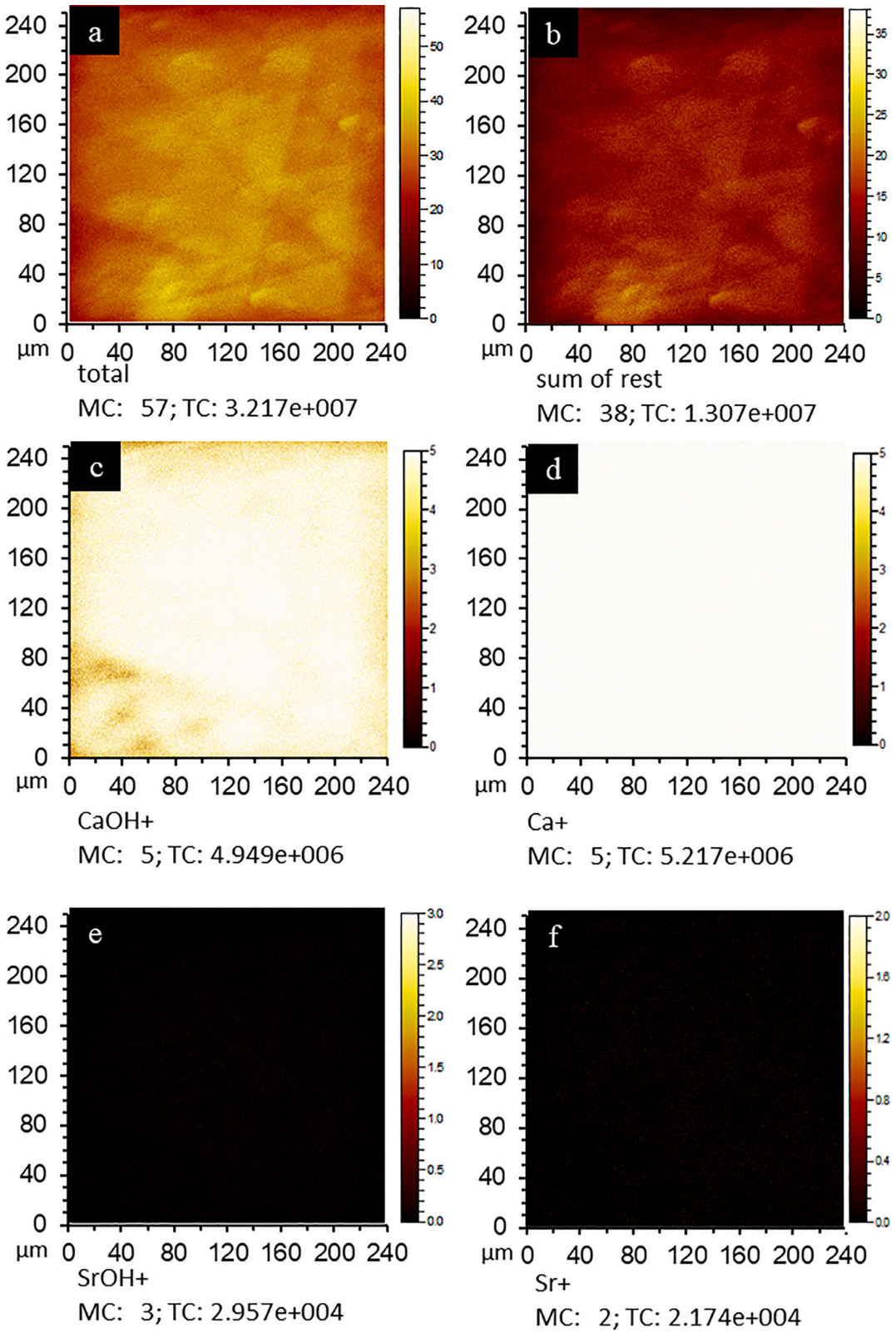

Fig. 3. ToF-SIMS pseudo-colour positive polarity ion mapping of a CaP coated ZEWX alloy showing the (a) total, (b) sum of the rest, (c) $CaOH^+$ (d) Ca^+ (e) $SrOH^+$ and (f) Sr^+ ion counts across a 250 × 250 µm area.

undergone significant dissolution which exposes the underlying alloy in places leading to its corrosion *via* the expected pitting process. The cracking observed is deemed to be a result of the drying process prior to analysis. The associated EDX elemental analysis data for the CaP and SrCaP coated Mg alloys post-immersion in SBF for 14 days is presented in Table 6 as atomic concentration (at. conc. (%)). When compared with the composition of the same samples before immersion in SBF (Table 4), the values for oxygen and carbon are both seen to increase, while those for calcium and magnesium are reduced which is consistent with the corrosion process. Finally, the phosphorous and strontium values for the

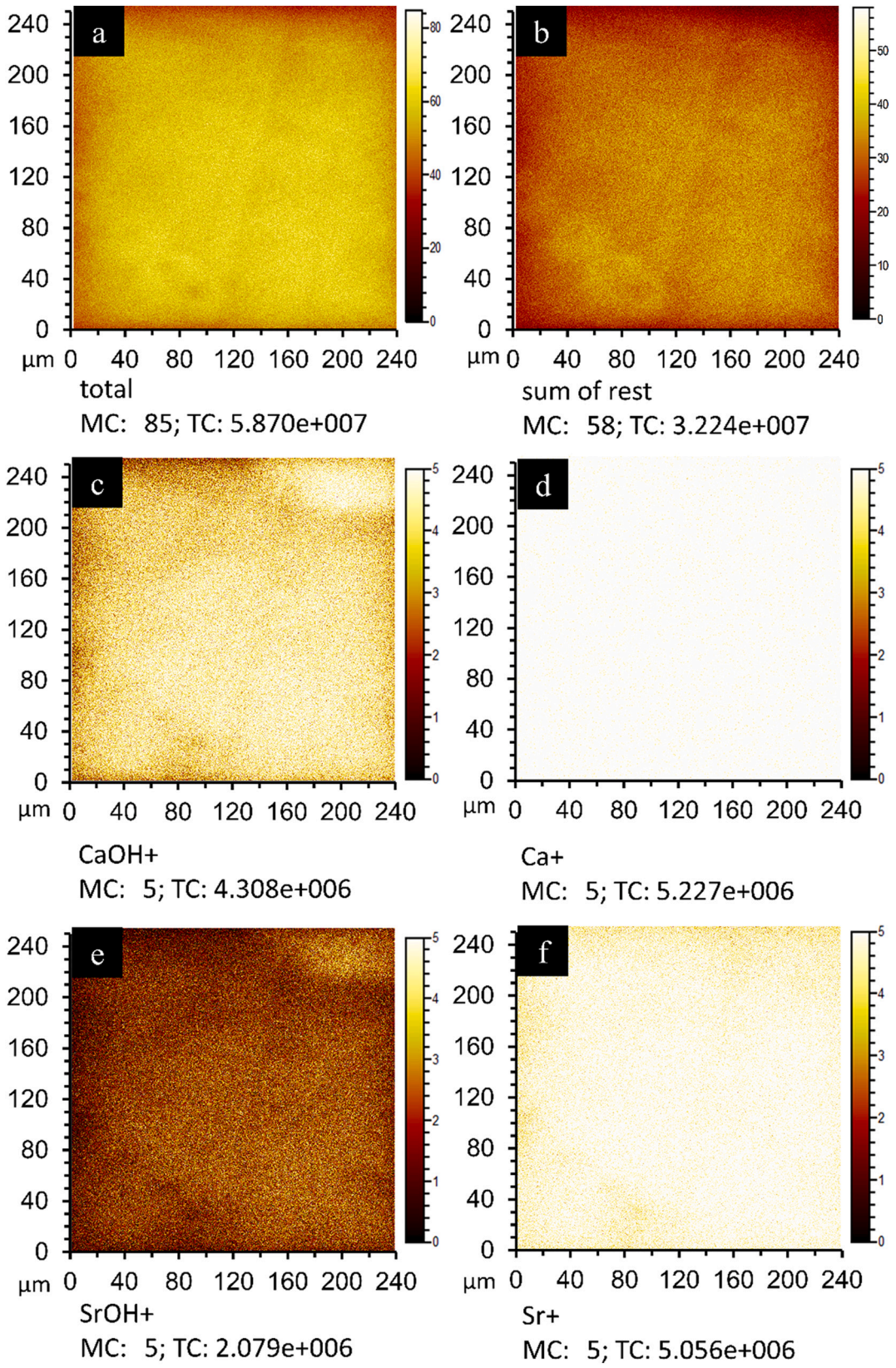

Fig. 4. ToF-SIMS pseudo-colour positive polarity ion mapping of a SrCaP coated ZEWX alloy showing the ion count for (a) total, (b) sum of rest, (c) $CaOH^+$ (d) Ca^+ (e) $SrOH^+$ and (f) Sr^+ peaks across a 250 × 250 µm area.

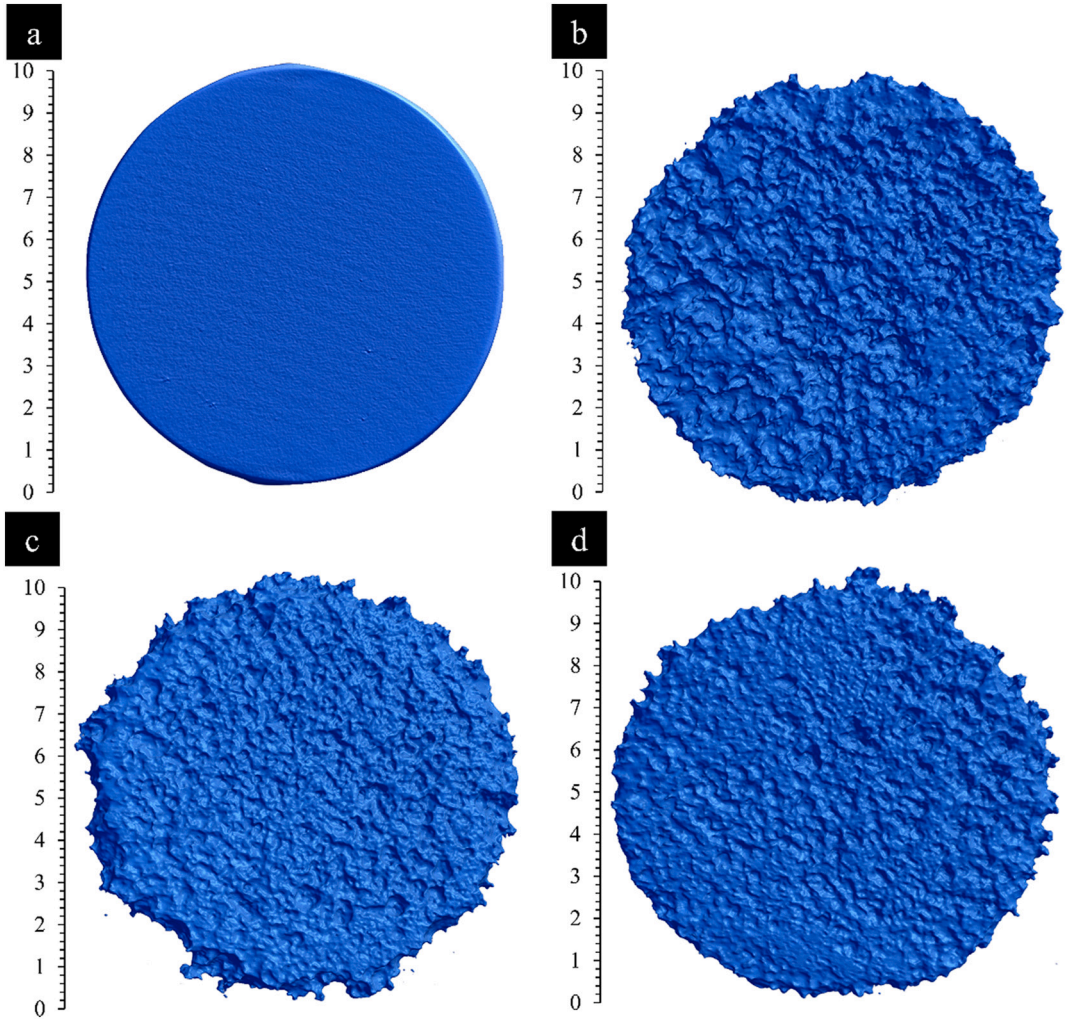

Fig. 5. μCT 3D volumetric reconstructions for (a) pristine WJK Mg alloy, pre-immersion and (b) uncoated, (c) CaP and (d) SrCaP sputter coated WJK alloys after immersion in SBF for 14 days. Scale bar = 10 mm.

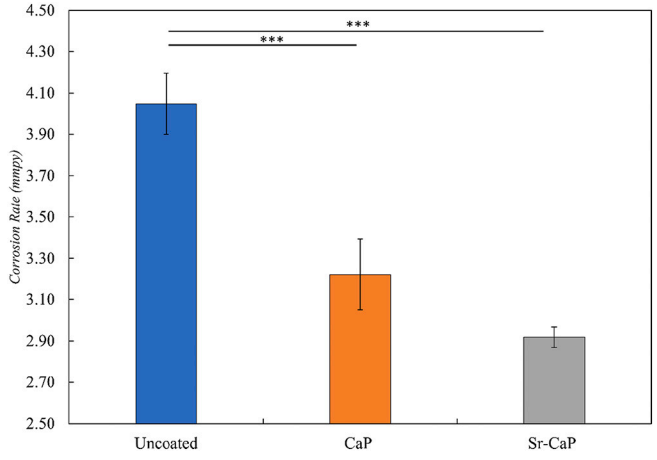

Fig. 6. Corrosion rate (mmpy) values determined by gravimetric analysis for uncoated, CaP coated and SrCaP coated WJK alloy substrates after immersion in SBF for 14-days: ***Statistical difference: Uncoated/CaP and Uncoated/SrCaP ($p < 0.001$).

Table 5
Total volume change for WJK and ZEWX Mg alloys with and without sputter deposited CaP and SrCaP coatings post-immersion in SBF for 14-days calculated by μCT 3D volumetric reconstruction.

	WJK	ZEWX
	Volume (mm^3)	Volume (mm^3)
Pre-immersion	71.2 ± 3.8	161.1 ± 16.4
	% volume loss after immersion in SBF	
Uncoated	40.3 ± 7.3	20.9 ± 12.8
CaP	29.1 ± 2.8	7.9 ± 8.1
SrCaP	29.1 ± 2.4	5.6 ± 15.9

coated samples show no significant change in concentration after exposure to SBF.

4. Discussion

SEM-EDX analysis of CaP and SrCaP coatings on ZEWX and WJK Mg alloy substrates indicate Ca/P ratios of 1.50 and 1.28, respectively while the Ca+Sr/P ratio for the latter sample is 1.56. These values are slightly lower than those expected for stoichiometric hydroxyapatite (1.67) and the 13% SrCaP (1.63) powder used to fabricate the latter sputter target. However, they are similar to those recorded previously for deposited RF sputtered amorphous CaP and SrCaP coatings on standard metal and

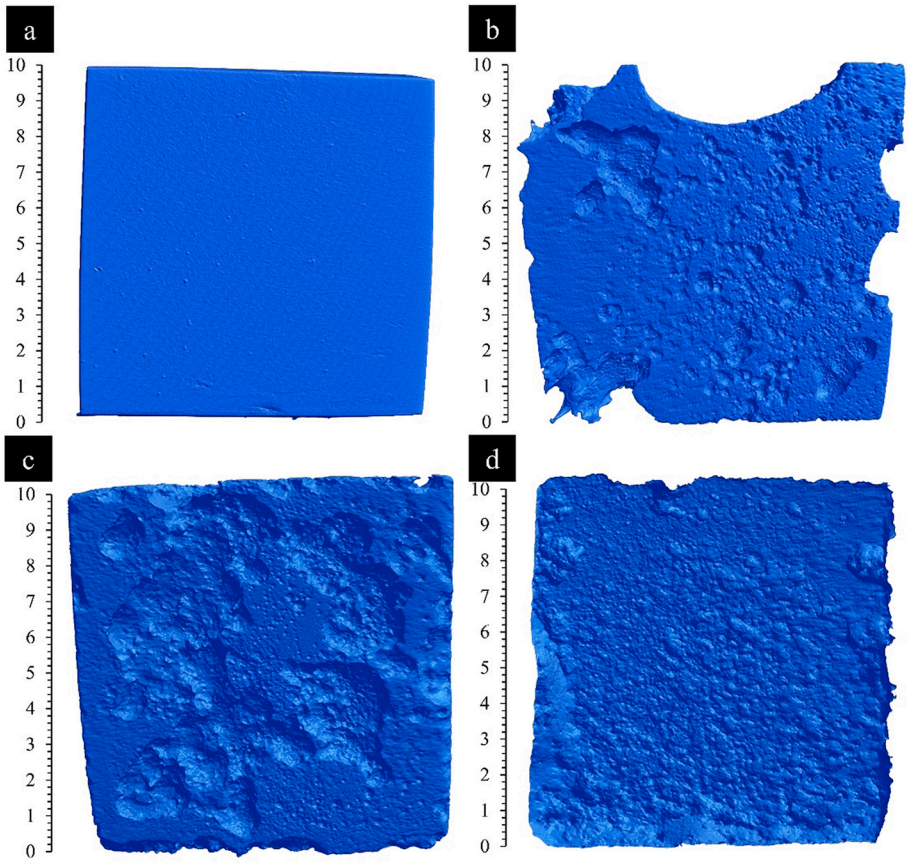

Fig. 7. μCT 3D volumetric reconstructions for (a) pristine alloy ZEWX alloy, pre-immersion and (b) uncoated, (c) CaP and (d) SrCaP sputter coated ZEWX alloys, after immersion in SBF for 14 days. Scale bar = 10 mm.

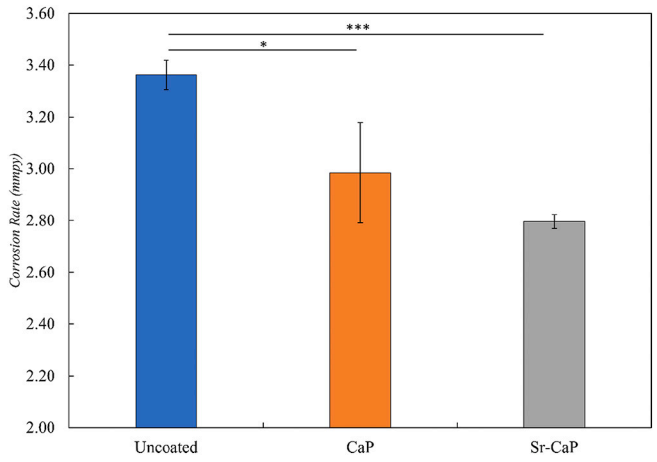

Fig. 8. Corrosion rate (mmpy) values determined by gravimetric analysis for uncoated, CaP and SrCaP coated ZEWX alloy substrates after immersion in SBF for 14 days. ***Statistical difference: Uncoated/CaP ($p < 0.1$); Uncoated/SrCaP ($p < 0.001$).

metal alloy substrates [24,27]. There are several possible reasons for these low Ca/P and Ca+Sr/P ratios, most importantly the use of dry pressed powders can lead to re-sputtering of the CaP and SrCaP onto the target surface as it is being used to deposit the materials onto the Mg alloy substrate [56,57]. In addition, the surface of the substrate is also known to have a significant influence on the growth mechanism of the coating by causing a gradation in composition. In this regard, given the abrasive pre-conditioning of the Mg alloys employed here it is likely that this effect contributes to the lower Ca/P and Ca+Sr/P ratios obtained for both coatings [58]. SEM micrographs for the CaP coated alloy samples (Fig. 1(e) and (f)) show the presence of globular features on the surface which are indicative of a semicrystalline calcium phosphate coating. The sputter deposited CaP and SrCaP materials both form conformal overlayers on the abraded alloy microstructure with no evidence of defects or delamination observed, which indicates that the coatings are well adhered. Given the difficulty in identifying such a thin film coating, EDX analysis was used to verify the presence of these sputter deposited coatings.

After immersion of the various CaP and SrCaP coated Mg alloys in SBF for 14 days, all samples exhibit corrosion products on the surface (Fig. 9), confirming that significant coating dissolution has occurred within the SBF solution leading to subsequent alloy corrosion. There is no evidence from the SEM images that the small amount of hydrogen evolution observed during alloy corrosion has had a significant effect on sample integrity at 14 days post immersion in SBF. SEM-EDX elemental analysis indicates an increase in the at. conc. (%) of oxygen and carbon on both substrates (Table 6) which can be attributed to the presence of carbonates within the SBF becoming entrapped on the surface. Interestingly, the at. conc. (%) for both the strontium and phosphate show no change post-immersion in SBF, while the calcium concentration decreases dramatically as seen in the changes to the Ca/P and Ca+Sr/P ratios observed. These data suggest that the as-deposited amorphous CaP coating undergoes significant dissolution over the 14-day period (with the phosphate detected here coming from SBF residues) but that the SrCaP coating is slightly more stable on both alloys under these conditions which is consistent with the behaviour observed in the respective SEM images (Fig. 9(c) and (d)).

ToF-SIMS ion mapping shows that the CaP and SrCaP coatings both have high counts of both Ca^+ and $CaOH^+$ ions with SrCaP containing the

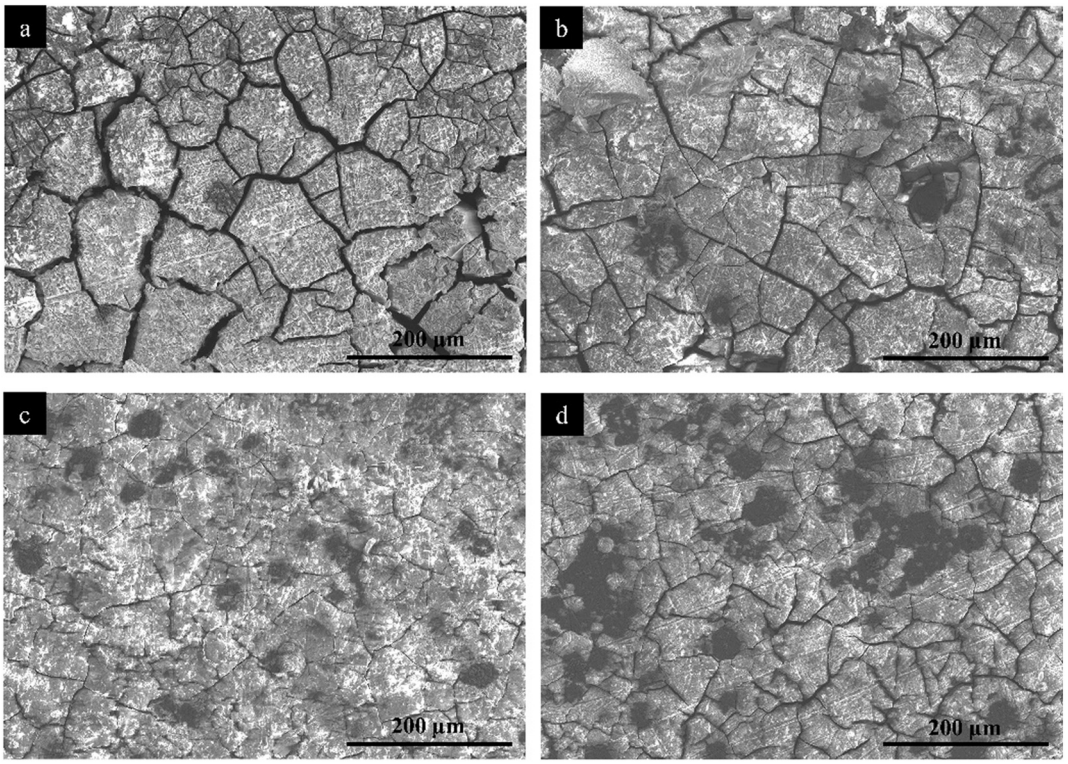

Fig. 9. SEM analysis (mag x200) of coated alloy samples post-immersion in SBF for 14 days with (a) WJK + CaP, (b) WJK + SrCaP, (c) ZEWX+CaP and (d) ZEWX+SrCaP. Scale bar = 200 µm.

Table 6
Atomic concentration (at. conc. (%)) values determined by SEM-EDX analysis for CaP and SrCaP coatings on WJK and ZEWX Mg alloys after immersion in SBF for 14 days.

Element	WJK+CaP	WJK+SrCaP	ZEWX+CaP	ZEWX+SrCaP
Oxygen	58.4 ± 0.6	51.5 ± 1.8	46.2 ± 2.8	56.1 ± 0.3
Carbon	13.1 ± 0.6	19.0 ± 2.7	33.1 ± 4.5	9.8 ± 0.8
Phosphorus	11.2 ± 0.6	12.0 ± 0.4	8.7 ± 0.7	11.1 ± 0.2
Strontium	0.0 ± 0.0	1.7 ± 0.3	0.0 ± 0.0	2.6 ± 0.1
Calcium	11.3 ± 0.3	11.7 ± 0.3	8.7 ± 0.7	12.1 ± 0.1
Magnesium	5.3 ± 0.4	3.3 ± 0.4	2.3 ± 0.3	7.2 ± 0.8
Sodium	0.5 ± 0.1	0.4 ± 0.0	1.0 ± 0.1	0.8 ± 0.0
Ca/P ratio	1.00	0.97	1.00	1.09
Ca + Sr/P	–	1.12	–	1.32

expected inclusion of Sr^{+} and $SrOH^{+}$ ions distributed evenly across the analysis area. This confirms that the RF magnetron sputter coatings produced in this study are both coherent and homogeneous which is consistent with findings from previous studies [59]. Pre-conditioning of the Mg alloy by manual abrasion results in identifiable striations that can be seen in the total and sum of rest ion maps. However, their presence does not appear to impact on the distribution of the individual ions within the sputter deposited CaP and SrCaP coatings which extend uniformly across both faces of the Mg alloy substrates.

Reconstructed µCT images show the extent of corrosion damage for WJK and ZEWX Mg alloys with and without CaP and SrCaP sputter coatings after 14 days in SBF at 37 °C. Although the composition of the Mg alloys has been tailored to increase corrosion resistance, they are still designed to be bioresorbable and demonstrate extensive pitting and volume loss (40.3% loss for WJK and 20.9% for ZEWX) post-immersion in SBF. It is noted that the volume loss for the pristine WJK alloy is nearly twice that measured for the ZEWX substrate. This considerable difference deemed to be mainly due to the respective alloy compositions. It is known that, irrespective of processing conditions, the overall change in corrosion rate arising from a change in alloy chemistry is the dominant consideration [60]. WJK alloys include 1 wt% Sr and 0.5 wt% Zr which are known to refine grain size and offer a degree of corrosion resistance [61,62] while the role of the 1 wt% Y is dependent on accompanying elements [63]. The ZEWX alloy also contains Y and Zr in slightly lower amounts, alongside 0.3 wt% Ca, 1 wt% Zn and 1 wt% rare earth metals (Nd/Gd) which have also been reported to increase corrosion resistance [64]. Therefore, the volume loss data reported here for the uncoated WJK and ZEWX alloys, is deemed to be due to these differences in the type and amount of the alloying elements.

This corrosion behaviour can, in part, be attributed to the static-dynamic [54] testing protocol employed, whereby the SBF media is changed daily such that a slightly elevated level of corrosion occurs when compared to standard static immersion studies. This method equates to 10 mL/cm^2 of SBF contacting the substrate, which when replenished daily is equivalent to a total of 140 mL/cm^2 over 14 days. It has been reported that this static-dynamic approach is closer to representation of *in vivo* conditions as it accounts for extracellular fluid exchange in the surrounding tissue environment. Previous studies that have used this approach report a lower corrosion rate [65,66] than seen here. However, the volume of media used in these studies were reported to be between 30 and 50 mL/cm^2 and so the difference in the corrosion rate for pristine samples here is attributable to this difference in testing. Application of a CaP coating results in a significant reduction in the rate and amount of corrosion, both visually and volumetrically; 29.1% loss for WJK + CaP and 7.9% loss for ZEWX+CaP. The pronounced reduction in volume loss seen for both types of CaP coated substrates is found to be significantly different ($p < 0.05$) when compared to that for the uncoated Mg alloys. The SrCaP coated WJK and ZEWX alloys also showed pitting across the sample surface with the volume loss values; 29.1% loss for WJK+SrCaP and 5.6% loss for ZEWX+SrCaP which are again significantly different ($p < 0.05$) compared to the uncoated Mg alloys. However, no significant difference was observed between the volume loss values for each of the CaP and SrCaP coated Mg alloys. This may be

attributed to the amorphous nature of both coatings in that they follow the same dissolution process, irrespective of ion substitution. It is notable that the standard deviation value for the volume loss data recorded for the ZEWX Mg CaP and SrCaP substrates is higher than for the equivalent WJK samples. This observation is consistent with the data for the pristine pre-immersion Mg alloys which may be as a result of their respective response to the sample preparation abrasion technique.

Calculation of corrosion rate (mmpy) reveals that the CaP and SrCaP coatings act to increase the corrosion resistance of the WJK and ZEWX Mg alloys, with the rate of corrosion falling in both cases; WJK to 3.22 ± 0.17 mmpy and ZEWX to 2.98 ± 0.19 mmpy with the application of the CaP coating. This is due to the coating acting as a barrier between the SBF and the underlying Mg alloy, until such times as the coating undergoes substantive dissolution to expose the underlying substrate. Incorporation of strontium within the CaP coating appears to reduce the corrosion rate further; WJK to 2.92 ± 0.05 mmpy and ZEWX to 2.79 ± 0.03 mmpy. However, as indicated above, there is no statistically significant difference between the CaP and SrCaP coating in this regard. There is currently a lack of literature reporting the effects of dissolution of amorphous Sr-substituted CaP coatings on Mg alloys, but it has been reported previously that amorphous coatings on titanium substrates generally undergo a high rate of dissolution [66] which differs from the behaviour reported here. The solubility of the SrCaP coatings is in large measure determined by the localised structural order of Sr within the CaP lattice [15], which is in part dependent on the underlying substrate. Additionally, the interfacial adhesion of the coating to the substrate can influence the solubility, whereby the local ordering of Sr-substituted CaP coatings on Mg alloys may be different to that of other metallic substrates, such as titanium. Although there is no statistically significant difference between the corrosion rates of CaP and SrCaP coatings here, the slightly increased corrosion resistance for the SrCaP coatings may be due to differences in localised ordering and interfacial adhesion influencing their solubility compared to that for the CaP thin films. The corrosion of SrCaP coated WJK and ZEWX clearly indicates that they both behave very much like the CaP coated Mg alloy specimens. This suggests that, whereas there may differences in the static dissolution rates of CaP and SrCaP sputter deposited coatings overall, the Mg alloy corrosion process is dominated by the dynamic element of the exposure to SBF.

The WJK and ZEWX coupons used here clearly have different shapes which influences the respective surface areas. The WJK disc substrates have a slightly lower surface area (~188.5 mm^2) than the square ZEWX coupons (~264 mm^2). Although the calculation of corrosion rate using Eq. (1) uses the nominal surface area, it does not account for the occurrence of defects and/or impurities which serve as nucleation points for the beginning of corrosion [2]. The difference in the surface area is therefore deemed not large enough to account for the significant change in corrosion rate and % volume loss observed between the two base alloy systems.

The results from this study indicate that incorporation of strontium into a calcium phosphate coating provides for enhanced corrosion resistance of the Mg alloys of interest when exposed to a static-dynamic environment that is equivalent to that offered by CaP alone. Such improvement in corrosion resistance is important to the mechanical properties of implantable orthopaedic devices fabricated from such magnesium alloys and studies are ongoing to determine the effects of such coatings on properties such as shear strength. Previous studies have reported that strontium can provide for positive effects on osseointegration and bone regeneration [67,68] which suggests that the RF magnetron sputtered SrCaP coatings used here could enhance the bioactivity of Mg alloys in a similar manner.

5. Conclusion

Sputter deposition of hydroxyapatite (HA) and strontium substituted hydroxyapatite powder targets (SrHA) has been shown to produce HA-like calcium phosphate coatings (CaP and SrCaP) on Mg alloys (WJK and ZEWX). The Ca/P ratio of the SrCaP coatings (as measured by SEM-EDX analysis) was 1.28 compared to a value of 1.50 for the CaP coatings. Both types of coating were found to improve Mg alloy corrosion resistance over a 14-day period of exposure to SBF. Volumetric reconstruction data (from μCT analysis) indicates that the SrCaP coating reduces the volume loss on each type of Mg alloy to an extent that is similar to the effects observed for the CaP layer. While the fully rendered μCT images presented here suggest that pitting is more pronounced on the CaP coatings compared to that of the SrCaP substrates, the interpretation of these data here is purely qualitative. No significant difference was observed in the quantitative corrosion rate between CaP and SrCaP substrates. Whereas, a statistically significant decrease in corrosion rate (calculated by gravimetric analysis) was observed between the uncoated Mg alloy substrates and both the CaP and SrCaP coated specimens individually. Hence, the application of soluble bioactive CaP and SrCaP coatings onto bioresorbable Mg alloys offers a means to control the rate of corrosion that occurs over the short to medium term. Moreover, while the addition of Sr to CaP coatings does not significantly alter the Mg alloy corrosion rate it does offer the potential to further enhance the attendant bioactivity.

Funding

Ulster University acknowledges funding from the Department for the Economy (DfE), Northern Ireland (Grant USI 111). University of Pittsburgh and North Carolina Agricultural and Technical State University acknowledge funding and the support *via* the National Science Foundation (NSF) funded Engineering Research Center for Revolutionizing Metallic Biomaterials (ERC-RMB) (Grant EEC-0812348).

CRediT authorship contribution statement

Conceptualization, J.G.A., S.McK., P.N.K, J.S. and B.J.M.; methodology, J.G.A, S.McK., A.R, Z.X, A.R.B, and P.L.; validation, J.G.A, S. McK., A.R.B and P.L.; formal analysis, J.G.A, S.McK., J.W, A.R.B and P. L.; investigation, J.G.A. and S.McK.; resources, A.R., Z.X., P.N.K, J.S. and B.J.M; data curation, J.G.A, S.McK. and J.W.; writing—original draft preparation, J.G.A. and J.W.; writing—review and editing, J.G.A., S. McK., J.W, A.R, Z.X., A.R.B., P.L., P.N.K, J.S. and B.J.M.; visualization, J. G.A, S.McK. and J.W.; supervision, P.N.K, J.S. and B.J.M.; project administration, P.N.K, J.S. and B.J.M.; funding acquisition, P.N.K, J.S. and B.J.M. All authors have read and agreed to the published version of the manuscript.

Declaration of competing interest

None.

Acknowledgments

The authors wish to acknowledge support for this work from a US-Ireland Centre-to-Centre R&D Partnership between Ulster University, North Carolina Agricultural and Technical State University, University of Pittsburgh, University of Cincinnati, Cincinnati Children's Hospital, and the National University of Ireland Galway. P.N.K. would also like to acknowledge the financial support from the Edward R. Weidlein Endowed Chair Professorship Funds, and the Center for Complex Engineered Multifunctional Materials (CCEMM) at the Swanson School of Engineering in the University of Pittsburgh for use of the equipment and instrumentation needed for preparing the alloys described herein.

References

[1] E.L. Boland, P. Ebrahimi, E.A. Gallagher, P. McGarry, A crystal plasticity-based investigation of fretting fatigue in bioresorbable magnesium elastic stable

intramedullary nails (ESINs), National University of Ireland, Galway, 2020. doi:10.31224/osf.io/kcjey.
[2] M. Esmaily, J.E. Svensson, S. Fajardo, N. Birbilis, G.S. Frankel, S. Virtanen, R. Arrabal, S. Thomas, L.G. Johansson, Fundamentals and advances in magnesium alloy corrosion, Prog. Mater. Sci. 89 (2017) 92–193, https://doi.org/10.1016/j.pmatsci.2017.04.011.
[3] Y.F. Zheng, X.N. Gu, F. Witte, Biodegradable metals, Mater. Sci. Eng. R. Rep. 77 (2014) 1–34, https://doi.org/10.1016/j.mser.2014.01.001.
[4] Y. Ding, C. Wen, P. Hodgson, Y. Li, Effects of alloying elements on the corrosion behavior and biocompatibility of biodegradable magnesium alloys: a review, J. Mater. Chem. B 2 (2014) 1912–1933, https://doi.org/10.1039/C3TB21746A.
[5] S. Agarwal, J. Curtin, B. Duffy, S. Jaiswal, Biodegradable magnesium alloys for orthopaedic applications: a review on corrosion, biocompatibility and surface modifications, Mater. Sci. Eng. C 68 (2016) 948–963, https://doi.org/10.1016/j.msec.2016.06.020.
[6] A. Abdal-hay, M. Dewidar, J. Lim, J.K. Lim, Enhanced biocorrosion resistance of surface modified magnesium alloys using inorganic/organic composite layer for biomedical applications, Ceram. Int. 40 (2014) 2237–2247, https://doi.org/10.1016/j.ceramint.2013.07.142.
[7] R. Surmenev, Radio Frequency Magnetron Sputter Deposition as a Tool for Surface Modification of Medical Implants, in: A. Vladescu (Ed.), IntechOpen, Rijeka, 2017: p. Ch. 12. doi:https://doi.org/10.5772/66396.
[8] G. Eddy Jai Poinern, S. Brundavanam, D. Fawcett, Biomedical Magnesium Alloys: A Review of Material Properties, Surface Modifications and Potential as a Biodegradable Orthopaedic Implant, Am. J. Biomed. Eng. 2 (2013) 218–240. doi:https://doi.org/10.5923/j.ajbe.20120206.02.
[9] X.-N. Gu, S.-S. Li, X.-M. Li, Y.-B. Fan, Magnesium based degradable biomaterials: a review, Front. Mater. Sci. 8 (2014) 200–218, https://doi.org/10.1007/s11706-014-0253-9.
[10] H.S. Brar, J. Wong, M.V. Manuel, Investigation of the mechanical and degradation properties of Mg–Sr and Mg–Zn–Sr alloys for use as potential biodegradable implant materials, J. Mech. Behav. Biomed. Mater. 7 (2012) 87–95, https://doi.org/10.1016/j.jmbbm.2011.07.018.
[11] R. Zeng, W. Dietzel, F. Witte, N. Hort, C. Blawert, Progress and challenge for magnesium alloys as biomaterials, Adv. Eng. Mater. 10 (2008) 3–14, https://doi.org/10.1002/adem.200800035.
[12] W.R. Zhou, Y.F. Zheng, M.A. Leeflang, J. Zhou, Mechanical property, biocorrosion and in vitro biocompatibility evaluations of Mg-Li-(Al)-(RE) alloys for future cardiovascular stent application, Acta Biomater. 9 (2013) 8488–8498, https://doi.org/10.1016/j.actbio.2013.01.032.
[13] C. Del Gaudio, P. Bagalà, M. Venturini, C. Grandi, P.P. Parnigotto, A. Bianco, G. Montesperelli, Assessment of in vitro temporal corrosion and cytotoxicity of AZ91D alloy, J. Mater. Sci. Mater. Med. 23 (2012) 2553–2562, https://doi.org/10.1007/s10856-012-4714-3.
[14] K. Chen, J. Dai, X. Zhang, Improvement of corrosion resistance of magnesium alloys for biomedical applications, Corros. Rev. 33 (2015) 101–117, https://doi.org/10.1515/corrrev-2015-0007.
[15] C. Capuccini, P. Torricelli, F. Sima, E. Boanini, C. Ristoscu, B. Bracci, G. Socol, M. Fini, I.N. Mihailescu, A. Bigi, Strontium-substituted hydroxyapatite coatings synthesized by pulsed-laser deposition: in vitro osteoblast and osteoclast response, Acta Biomater. 4 (2008) 1885–1893, https://doi.org/10.1016/j.actbio.2008.05.005.
[16] I. Pereiro, C. Rodríguez-Valencia, C. Serra, E.L. Solla, J. Serra, P. González, Pulsed laser deposition of strontium-substituted hydroxyapatite coatings, Appl. Surf. Sci. 258 (2012) 9192–9197, https://doi.org/10.1016/j.apsusc.2012.04.063.
[17] P. Yin, F. Feng, T. Lei, X. Jian, Colloidal-sol gel derived biphasic FHA/SrHA coatings, Surf. Coat. Technol. 207 (2012) 608–613, https://doi.org/10.1016/j.surfcoat.2012.08.006.
[18] A. Roy, S.S. Singh, M.K. Datta, B. Lee, J. Ohodnicki, P.N. Kumta, Novel sol–gel derived calcium phosphate coatings on Mg4Y alloy, Mater. Sci. Eng. B 176 (2011) 1679–1689, https://doi.org/10.1016/j.mseb.2011.08.007.
[19] M. Catauro, F. Barrino, I. Blanco, S. Piccolella, S. Pacifico, Use of the Sol–Gel Method for the Preparation of Coatings of Titanium Substrates with Hydroxyapatite for Biomedical Application, Coatings. 10 (2020), 10, 203. doi:https://doi.org/10.3390/coatings10030203.
[20] M. Qadir, Y. Li, K. Munir, C. Wen, Calcium phosphate-based composite coating by micro-arc oxidation (MAO) for biomedical application: a review, Crit. Rev. Solid State Mater. Sci. 43 (2018) 392–416, https://doi.org/10.1080/10408436.2017.1358148.
[21] Y. Chen, J. Dou, Z. Pang, Z. Zheng, H. Yu, C. Chen, Ag-containing antibacterial self-healing micro-arc oxidation coatings on Mg–Zn–Sr alloys, Surf. Eng. (2020) 1–16, https://doi.org/10.1080/02670844.2020.1800346.
[22] Y. Wang, X. Li, M. Chen, Y. Zhao, C. You, Y. Li, G. Chen, In vitro and in vivo degradation behavior and biocompatibility evaluation of microarc oxidation-fluoridated hydroxyapatite-coated Mg–Zn–Zr–Sr alloy for bone application, ACS Biomater Sci. Eng. 5 (2019) 2858–2876, https://doi.org/10.1021/acsbiomaterials.9b00564.
[23] A.R. Boyd, B.J. Meenan, N.S. Leyland, Surface characterisation of the evolving nature of radio frequency (RF) magnetron sputter deposited calcium phosphate thin films after exposure to physiological solution, Surf. Coat. Technol. (2006), https://doi.org/10.1016/j.surfcoat.2005.09.032.
[24] A.R. Boyd, L. Rutledge, L.D. Randolph, I. Mutreja, B.J. Meenan, The deposition of strontium-substituted hydroxyapatite coatings, J. Mater. Sci. Mater. Med. 26 (2015) 65, https://doi.org/10.1007/s10856-014-5377-z.
[25] J.G. Acheson, S. McKillop, P. Lemoine, A.R. Boyd, B.J. Meenan, Control of magnesium alloy corrosion by bioactive calcium phosphate coating: implications for resorbable orthopaedic implants, Materialia. 6 (2019) 10, https://doi.org/10.1016/j.mtla.2019.100291.
[26] A.R. Boyd, L. Rutledge, L.D. Randolph, B.J. Meenan, Strontium-substituted hydroxyapatite coatings deposited via a co-deposition sputter technique, Mater. Sci. Eng. C 46 (2015) 290–300, https://doi.org/10.1016/j.msec.2014.10.046.
[27] M. Razavi, M. Fathi, O. Savabi, S. Mohammad Razavi, B. Hashemi Beni, D. Vashaee, L. Tayebi, Controlling the degradation rate of bioactive magnesium implants by electrophoretic deposition of akermanite coating, Ceram. Int. 40 (2014) 3865–3872, https://doi.org/10.1016/j.ceramint.2013.08.027.
[28] H. Hornberger, S. Virtanen, A.R. Boccaccini, Biomedical coatings on magnesium alloys - a review, Acta Biomater. 8 (2012) 2442–2455, https://doi.org/10.1016/j.actbio.2012.04.012.
[29] H.M. Mousa, A.P. Tiwari, J. Kim, S.P. Adhikari, C.H. Park, C.S. Kim, A novel in situ deposition of hydroxyapatite nanoplates using anodization/hydrothermal process onto magnesium alloy surface towards third generation biomaterials, Mater. Lett. 164 (2016) 144–147, https://doi.org/10.1016/j.matlet.2015.10.145.
[30] C.P. Yoganand, V. Selvarajan, V. Cannillo, A. Sola, E. Roumeli, O.M. Goudouri, K. M. Paraskevopoulos, M. Rouabhia, Characterization and in vitro-bioactivity of natural hydroxyapatite based bio-glass–ceramics synthesized by thermal plasma processing, Ceram. Int. 36 (2010) 1757–1766, https://doi.org/10.1016/j.ceramint.2010.02.048.
[31] H.-M. Kim, Ceramic bioactivity and related biomimetic strategy, Curr. Opin. Solid State Mater. Sci. 7 (2003) 289–299, https://doi.org/10.1016/j.cossms.2003.09.014.
[32] Y. Su, D. Li, Y. Su, C. Lu, L. Niu, J. Lian, G. Li, Improvement of the biodegradation property and biomineralization ability of magnesium–hydroxyapatite composites with dicalcium phosphate dihydrate and hydroxyapatite coatings, ACS Biomater Sci. Eng. 2 (2016) 818–828, https://doi.org/10.1021/acsbiomaterials.6b00013.
[33] C.Y. Li, X.L. Fan, R.C. Zeng, L.Y. Cui, S.Q. Li, F. Zhang, Q.K. He, M.B. Kannan, H.W. (George) Jiang, D.C. Chen, S.K. Guan, Corrosion resistance of in-situ growth of nano-sized Mg(OH) 2 on micro-arc oxidized magnesium alloy AZ31—Influence of EDTA, J. Mater. Sci. Technol. 35 (2019) 1088–1098. doi:https://doi.org/10.1016/j.jmst.2019.01.006.
[34] R.A. Surmenev, M.A. Surmeneva, I.Y. Grubova, R.V. Chernozem, B. Krause, T. Baumbach, K. Loza, M. Epple, RF magnetron sputtering of a hydroxyapatite target: a comparison study on polytetrafluorethylene and titanium substrates, Appl. Surf. Sci. 414 (2017) 335–344, https://doi.org/10.1016/j.apsusc.2017.04.090.
[35] M.M. McCafferty, G.A. Burke, B.J. Meenan, Calcium phosphate thin films enhance the response of human mesenchymal stem cells to nanostructured titanium surfaces, J. Tissue Eng. 5 (2014) 204173141453751. doi:https://doi.org/10.1177/2041731414537513.
[36] L. Robinson, K. Salma-Ancane, L. Stipniece, B.J. Meenan, A.R. Boyd, The deposition of strontium and zinc Co-substituted hydroxyapatite coatings, J. Mater. Sci. Mater. Med. 28 (2017) 51, https://doi.org/10.1007/s10856-017-5846-2.
[37] M.M. McCafferty, G.A. Burke, B.J. Meenan, Mesenchymal stem cell response to conformal sputter deposited calcium phosphate thin films on nanostructured titanium surfaces, J. Biomed. Mater. Res. A 102 (2014) 3585–3597, https://doi.org/10.1002/jbm.a.35018.
[38] M.S. Uddin, C. Hall, P. Murphy, Surface treatments for controlling corrosion rate of biodegradable Mg and Mg-based alloy implants, Sci. Technol. Adv. Mater. 16 (2015) 53501, https://doi.org/10.1088/1468-6996/16/5/053501.
[39] N. Lowry, Y. Han, B.J. Meenan, A.R. Boyd, Strontium and zinc co-substituted nanophase hydroxyapatite, Ceram. Int. 43 (2017) 12070–12078, https://doi.org/10.1016/j.ceramint.2017.06.062.
[40] F. Ren, R. Xin, X. Ge, Y. Leng, Characterization and structural analysis of zinc-substituted hydroxyapatites, Acta Biomater. 5 (2009) 3141–3149, https://doi.org/10.1016/j.actbio.2009.04.014.
[41] N. Lowry, M. Brolly, Y. Han, S. McKillop, B.J. Meenan, A.R. Boyd, Synthesis and characterisation of nanophase hydroxyapatite co-substituted with strontium and zinc, Ceram. Int. 44 (2018) 7761–7770, https://doi.org/10.1016/j.ceramint.2018.01.206.
[42] C.T. Wong, W.W. Lu, W.K. Chan, K.M.C. Cheung, K.D.K. Luk, D.S. Lu, A.B.M. Rabie, L.F. Deng, J.C.Y. Leong, In vivo cancellous bone remodeling on a strontium-containing hydroxyapatite (sr-HA) bioactive cement, J. Biomed. Mater. Res. A 68A (2004) 513–521, https://doi.org/10.1002/jbm.a.20089.
[43] G.X. Ni, W.W. Lu, K.Y. Chiu, Z.Y. Li, D.Y.T. Fong, K.D.K. Luk, Strontium-containing hydroxyapatite (Sr-HA) bioactive cement for primary hip replacement: an in vivo study, J. Biomed. Mater. Res. B Appl. Biomater. 77B (2006) 409–415, https://doi.org/10.1002/jbm.b.30417.
[44] L. Stipniece, S. Wilson, J.M. Curran, R. Chen, K. Salma-Ancane, P.K. Sharma, B. J. Meenan, A.R. Boyd, Strontium substituted hydroxyapatite promotes direct primary human osteoblast maturation, Ceram. Int. (2020), https://doi.org/10.1016/j.ceramint.2020.09.182.
[45] E. Landi, S. Sprio, M. Sandri, G. Celotti, A. Tampieri, Development of Sr and CO3 co-substituted hydroxyapatites for biomedical applications, Acta Biomater. 4 (2008) 656–663, https://doi.org/10.1016/j.actbio.2007.10.010.
[46] M. Schumacher, A. Lode, A. Helth, M. Gelinsky, A novel strontium(II)-modified calcium phosphate bone cement stimulates human-bone-marrow-derived mesenchymal stem cell proliferation and osteogenic differentiation in vitro, Acta Biomater. 9 (2013) 9547–9557, https://doi.org/10.1016/j.actbio.2013.07.027.
[47] X. Gu, W. Lin, D. Li, H. Guo, P. Li, Y. Fan, Degradation and biocompatibility of a series of strontium substituted hydroxyapatite coatings on magnesium alloys, RSC Adv. 9 (2019) 15013–15021, https://doi.org/10.1039/c9ra02210d.
[48] D. Zhao, W. Shi, P. Shang, H. Nie, Y. Zhang, J. Tang, Effects of Sr incorporation on surface structure and corrosion resistance of hydroxyapatite coated Mg-4Zn alloy

for biomedical applications, Trans. Nonferrous Met. Soc. Chin. 28 (2018) 1563–1570, https://doi.org/10.1016/S1003-6326(18)64798-3.
[49] L. Liu, K. Gebresellasie, B. Collins, H. Zhang, Z. Xu, J. Sankar, Y.C. Lee, Y. Yun, Degradation rates of pure zinc, magnesium, and magnesium alloys measured by volume loss, mass loss, and hydrogen evolution, Appl. Sci. 8 (2018). doi:https://doi.org/10.3390/app8091459.
[50] D. Rohanová, D. Horkavcová, A. Helebrant, A.R. Boccaccini, Assessment of in vitro testing approaches for bioactive inorganic materials, J. Non-Cryst. Solids 432 (2016) 53–59, https://doi.org/10.1016/j.jnoncrysol.2015.03.016.
[51] C.E. Smith, Z. Xu, J. Waterman, J. Sankar, Cytocompatibility assessment of MgZnCa alloys, Emerg. Mater. Res. 2 (2013) 283–290, https://doi.org/10.1680/emr.13.00026.
[52] T. Kokubo, H. Takadama, How useful is SBF in predicting in vivo bone bioactivity? Biomaterials. 27 (2006) 2907–2915, https://doi.org/10.1016/j.biomaterials.2006.01.017.
[53] H.-M. Kim, T. Himeno, M. Kawashita, T. Kokubo, T. Nakamura, The mechanism of biomineralization of bone-like apatite on synthetic hydroxyapatite: an in vitro assessment, J. R. Soc. Interface 1 (2004) 17–22, https://doi.org/10.1098/rsif.2004.0003.
[54] D. Rohanová, D. Horkavcová, L. Paidere, A.R. Boccaccini, P. Bozděchová, P. Bezdička, Interaction of HEPES buffer with glass-ceramic scaffold: can HEPES replace TRIS in SBF? J. Biomed. Mater. Res. B Appl. Biomater. 106 (2018) 143–152, https://doi.org/10.1002/jbm.b.33818.
[55] ASTM G1-90, ASTM G1 Standard Practice for Preparing, Cleaning, and Evaluation Corrosion Test Specimens, Astm. (2003) 8. https://www.astm.org/DATABASE.CART/HISTORICAL/G1-03R11.htm.
[56] B. Feddes, J.G.C. Wolke, J.A. Jansen, A.M. Vredenberg, Radio frequency magnetron sputtering deposition of calcium phosphate coatings: the effect of resputtering on the coating composition, J. Appl. Phys. 93 (2003) 9503–9507, https://doi.org/10.1063/1.1576894.
[57] M.A. Surmeneva, A. Kovtun, A. Peetsch, S.N. Goroja, A.A. Sharonova, V. F. Pichugin, I.Y. Grubova, A.A. Ivanova, A.D. Teresov, N.N. Koval, V. Buck, A. Wittmar, M. Ulbricht, O. Prymak, M. Epple, R.A. Surmenev, Preparation of a silicate-containing hydroxyapatite-based coating by magnetron sputtering: structure and osteoblast-like MG63 cells in vitro study, RSC Adv. 3 (2013) 11240, https://doi.org/10.1039/c3ra40446c.
[58] R.A. Surmenev, A review of plasma-assisted methods for calcium phosphate-based coatings fabrication, Surf. Coat. Technol. 206 (2012) 2035–2056, https://doi.org/10.1016/j.surfcoat.2011.11.002.
[59] J.G. Acheson, L. Robinson, S. McKillop, S. Wilson, M.J. McIvor, B.J. Meenan, A. R. Boyd, TOFSIMS and XPS characterisation of strontium in amorphous calcium phosphate sputter deposited coatings, Mater. Charact. 110739 (2020), https://doi.org/10.1016/j.matchar.2020.110739.
[60] X. Xia, C.H.J. Davies, J.F. Nie, N. Birbilis, Influence of composition and processing on the corrosion of magnesium alloys containing binary and ternary additions of zinc and strontium, CORROSION. 71 (2015) 38–49, https://doi.org/10.5006/1417.
[61] X.N. Gu, X.H. Xie, N. Li, Y.F. Zheng, L. Qin, In vitro and in vivo studies on a mg–Sr binary alloy system developed as a new kind of biodegradable metal, Acta Biomater. 8 (2012) 2360–2374, https://doi.org/10.1016/j.actbio.2012.02.018.
[62] U. Riaz, I. Shabib, W. Haider, The current trends of mg alloys in biomedical applications—a review, J. Biomed. Mater. Res. B Appl. Biomater. 107 (2019) 1970–1996, https://doi.org/10.1002/jbm.b.34290.
[63] I. Johnson, H. Liu, A study on factors affecting the degradation of magnesium and a magnesium-yttrium alloy for biomedical applications, PLoS One 8 (2013), e65603, https://doi.org/10.1371/journal.pone.0065603.
[64] X. Xia, J.F. Nie, C.H.J. Davies, W.N. Tang, S.W. Xu, N. Birbilis, The influence of low levels of zinc, calcium, gadolinium, strontium, and zirconium on the corrosion of magnesium for wrought applications, CORROSION. 71 (2015) 1370–1386, https://doi.org/10.5006/1802.
[65] D.T. Chou, D. Hong, P. Saha, J. Ferrero, B. Lee, Z. Tan, Z. Dong, P.N. Kumta, In vitro and in vivo corrosion, cytocompatibility and mechanical properties of biodegradable Mg-Y-Ca-Zr alloys as implant materials, Acta Biomater. 9 (2013) 8518–8533, https://doi.org/10.1016/j.actbio.2013.06.025.
[66] G. Graziani, M. Boi, M. Bianchi, A review on ionic substitutions in hydroxyapatite thin films: towards complete biomimetism, Coatings 8 (2018), https://doi.org/10.3390/coatings8080269.
[67] V. Aina, L. Bergandi, G. Lusvardi, G. Malavasi, F.E. Imrie, I.R. Gibson, G. Cerrato, D. Ghigo, Sr-containing hydroxyapatite: morphologies of HA crystals and bioactivity on osteoblast cells, Mater. Sci. Eng. C 33 (2013) 1132–1142, https://doi.org/10.1016/j.msec.2012.12.005.
[68] J. Abert, C. Bergmann, H. Fischer, Wet chemical synthesis of strontium-substituted hydroxyapatite and its influence on the mechanical and biological properties, Ceram. Int. 40 (2014) 9195–9203, https://doi.org/10.1016/j.ceramint.2014.01.138.